IJAME

Int. J. of Applied Mechanics and Engineering, ???, vol.???, No.???, pp.???-???
DOI: 10.59441/ijame/220435

EFFECT OF ANNULAR FIN GEOMETRY ON THERMO-HYDRAULIC CHARACTERISTICS OF ROUND HEAT SINKS: AN EXPERIMENTAL STUDY

Z.A. Salih[1] and E.F. Abbas[*2]
[1]Mechanical Power Techniques Engineering Department, Renewable Energy Research Centre, Northern Technical University, IRAQ
[2]Mechanical Power Technical Eng., Northern Technical University, Technical Engineering College/ Kirkuk, IRAQ
E-mail: ehsanfadhil@ntu.edu.iq

This study experimentally investigates the influence of annular fin geometry on thermo-hydraulic performance under crossflow forced-convection conditions. Four heat sink configurations – a constant cross-section fin, a stepped fin, a modified stepped fin, and a triangular fin – were tested using an open-channel rig over 36 operating conditions formed by three air velocities $(2-6\,m/s)$ and three electrical input powers $(13-39W)$. The results show that the Nusselt number increases with Reynolds number for all geometries, with average enhancements of approximately $10-15\%$, $20-25\%$, and $30-35\%$ for the stepped, modified stepped, and triangular fins, respectively, compared to the baseline. Pressure drop also increased with Reynolds number, with the modified stepped fin exhibiting the highest penalty, while the triangular fin maintained a more moderate increase. At fixed Reynolds numbers, the effect of input power was secondary, confirming the dominance of flow inertia and geometry. Geometry-specific Nusselt number correlations with coefficients of determination exceeding 0.95 were developed, and the analytical model for the baseline fin was validated against experimental data with deviations below 2% .

Key words: heat sink, heat transfer enhancement, annular fin, round heat sink.

1. Introduction

Heat sinks, specialized heat exchangers, are used to dissipate excess thermal energy from high-power devices that cannot independently regulate their Temperature. By facilitating heat transfer to an adjacent fluid medium, they help prevent overheating and potential system failure. Their functionality is grounded in principles such as conduction, convection, and radiation, and is often enhanced by the inclusion of extended surfaces, such as fins and spines. Commonly found in electronics, refrigeration, and heat engines, heat sinks are typically made up of arrays of metallic fins. Their performance can be optimized by increasing surface area, enhancing thermal conductivity, or improving the heat transfer coefficient, thereby ensuring effective and reliable thermal management [1, 2]. A heat sink is a passive cooling component that consists of a base plate for heat absorption, along with extended surfaces such as fins or pins that increase the area for heat dissipation. Often, thermal interface materials are employed to minimize thermal resistance. More sophisticated designs may incorporate heat pipes or vapor chambers to enhance heat transfer efficiency and ensure device reliability. Between 1900 and 1920, the use of heat sink heating became widely recognized in factories and esteemed social venues, such as churches and theaters. This burgeoning demand spurred the development of multi-column cast-iron relief heat sinks, which offered enhanced heat dissipation and enabled heating larger buildings. The 1920s and 1930s witnessed a technological revolution with the advent of single-column steel heat sinks, representing a significant leap forward in thermal management design and efficiency

[*] To whom correspondence should be addressed

[3, 4]. In recent decades, a variety of fin geometries and configurations, such as straight, annular, and perforated fins, have been proposed and studied to enhance heat transfer while minimizing pressure drop. Previous research has demonstrated that both the shape and arrangement of fins significantly influence the overall heat transfer coefficient and thermal resistance in heat exchangers. However, despite extensive studies on various fin designs, there remains a noticeable gap in comprehensive experimental and theoretical investigations of specific fin geometries under conditions that do not involve annular heat sinks. Annular fins are commonly used to improve heat transfer from cylindrical surfaces. These fins are attached externally to circular pipes, which increases the heat transfer rate by expanding the effective surface area. Due to their widespread use, significant efforts have been made to modify the shapes of these fins to optimize material utilization. In the case of constant cross-sectional annular fins, the material near the tip contributes less to conductive heat transfer. This has led to the exploration of various tapered profiles, such as triangular, trapezoidal, parabolic, and hyperbolic designs. When considering both cost-effectiveness and heat transfer efficiency, designers aim to identify the optimal fin profile for a specific fin volume [4]. Over the past two decades, extensive research has been devoted to the investigation of ringed fins. The majority of these contributions have been theoretical, with limited experimental validation to substantiate the proposed models. Representative studies in this domain are: In 1965, Brown [5] derived analytical expressions to optimize uniform annular fins for maximum heat transfer while maintaining a fixed fin volume. His work relates the inner radius (r_1), outer radius (r_2), and thickness (δ) of the fins. These findings offer essential guidance for designing efficient annular fins in thermal systems. Buccini and Soliman [6] analyzed the dimensions of annular fins to maximize heat dissipation. They utilized one-dimensional conduction and convection to minimize thermal resistance and provide design guidelines for enhanced thermal performance. Lalot *et al*. [7] developed an analytical model to evaluate annular fins made from two different materials, such as a high-conductivity coating applied over a base material. The study produced formulas for temperature distribution and fin efficiency, demonstrating that these coatings significantly enhance efficiency by minimizing temperature gradients. This work provides valuable guidance for optimizing fin design in thermal systems. Mokheimer [8] studied annular fins with various profiles, including rectangular, triangular, concave, and convex parabolic shapes, under natural convection with locally varying heat transfer coefficients. Using plate-convection correlations, the study calculated fin efficiency and presented the results as curves of radius ratio and dimensionless parameters. The findings emphasize that spatial variation in the heat transfer coefficient significantly affects fin efficiency, underscoring its importance in the thermal analysis of annular fins. Mon and Gross [9] conducted a numerical investigation into the effects of fin spacing in annular-finned tube heat exchangers. Their computational results highlighted the crucial role of fin spacing in shaping airflow patterns, heat transfer rates, and pressure drops. They identified the optimal spacing needed to balance thermal enhancement and hydraulic performance, offering practical guidance for the efficient design of annular-finned tube heat exchangers. Arslanturk [10] developed correlation equations to optimize the uniform thickness of annular fins. By fixing the fins' volume, the study identified dimensionless geometric parameters that maximize heat transfer. It expressed the optimal radius ratio as a function of the Bi number and fin volume. These correlations serve as a valuable guide for engineers in designing fins that enhance heat dissipation efficiency. Naphon [10] conducted a theoretical study on annular fins under three conditions: dry, partially wet, and fully wet. Using energy and mass conservation principles along with the finite difference method, the results indicated that the surface condition significantly affects performance. Fully wet fins demonstrated the highest efficiency, providing valuable insights for the design of heat exchangers and electronic cooling systems. Sharqawy and Zubair [11] present an analytical solution for assessing the efficiency and optimizing annular fins under combined heat and mass transfer conditions. Their model integrates diffusion effects with thermal conduction to establish performance criteria. The results emphasize the significance of fin geometry and transfer coefficients in maximizing efficiency, providing a theoretical foundation for optimizing annular fin design in humid environments. Aziz and Fong [12] analyze annular fins with two boundary conditions: (a) simultaneous base temperature and heat flux, and (b) fixed base and tip temperatures. They develop analytical solutions to assess temperature distribution, fin efficiency, and heat transfer rates, offering insights for optimizing fin performance under varying thermal constraints. Nagarani *et al.* [13] optimized elliptical annular fins using a genetic algorithm, focusing on parameters like major and

minor axes, thermal conductivity, and convection coefficient. Their study found that optimal geometries enhance heat dissipation and reduce material use, with elliptical fins outperforming traditional circular fins and offering a systematic design for compact heat exchangers. Moinuddin *et al*. [14] analyzed Heat and mass transfer in annular fins with varying cross-sectional areas, aiming to determine their optimal dimensions. Through analytical modeling, the study established criteria for maximizing fin efficiency while minimizing material usage. The results provide design guidelines for selecting appropriate fin geometries, thereby improving the performance of annular fins in heat- and mass-transfer applications. Huang and Chung [15] developed an iterative regularization algorithm based on the conjugate gradient method to determine the optimal shapes for fully wet annular fins. By considering temperature-dependent properties and Bi numbers, their study identified fin geometries that maximize thermal efficiency and improve heat transfer performance. Kundu *et al*. [16] propose an approximate analytical method for the optimal design of annular step fins. Their approach simplifies the temperature distribution equation into an exponential form, making it easier to determine the fin dimensions that maximize heat transfer efficiency. This method helps engineers optimize fin geometry to enhance thermal performance. Kunda and Lee [17] developed an analytical framework for evaluating the thermal performance of annular-step porous fins. By incorporating porosity effects into the heat transfer model, the study derives optimal conditions for maximizing heat dissipation. The analysis highlights the benefits of porous structures in enhancing fin efficiency and provides valuable guidelines for designing high-performance extended surfaces in thermal systems. Chen *et al*. [18] demonstrate that fin geometry and spacing have a significant impact on natural convection heat transfer in vertical annular finned-tube heat exchangers. This conclusion is supported by strong agreement between numerical simulations and experimental validation. The findings provide insights for optimizing the design of finned-tube heat exchangers under natural convection conditions. Yuan *et al.* [19] evaluate existing prediction methods for the heat transfer coefficient in annular flow and identify their limitations under different conditions. Through comprehensive analysis and validation, they propose a novel correlation to improve accuracy across a wide operating range. This new model enhances predictive capability, providing a reliable tool for thermal system design and engineering applications. Yang *et al.* [20] propose a design approach for annular fins that are non-uniformly distributed in shell-and-tube thermal energy storage units. Their numerical analysis shows that customized fin spacing improves heat transfer, reduces thermal resistance, and enhances charging and discharging rates. The findings emphasize the benefits of a non-uniform fin distribution over traditional uniform designs, offering practical strategies to optimize the performance of thermal energy storage systems. Sarwe and Kulkarni [21] employed the differential transformation method (DTM) to investigate annular fins with variable thermal conductivity. The DTM effectively predicted the temperature distribution and fin efficiency. The results were validated against both analytical and finite-difference methods, confirming the DTM's reliability for analyzing annular-fin performance. Tahrour *et al.* [22] conducted a 3D computational fluid dynamics (CFD) analysis on various annular finned-tube designs, including concentric, eccentric, perforated, serrated, and star-shaped configurations. Their findings revealed that the star-shaped fin achieved the highest overall performance, while the eccentric circular fin provided the best balance between heat transfer and pressure drop. These insights are valuable for optimizing heat exchangers.

Previous studies have optimized annular fins through analytical models, coatings, variable profiles, spacing, and advanced numerical methods, often supported by CFD but with limited experimental validation. Consequently, a gap remains in comprehensive experimental investigations linking annular fin geometry to thermo-hydraulic performance under practical conditions. Addressing this gap, the present study experimentally examines the thermo-hydraulic characteristics of an annular fin heat sink under forced convection, considering varying airflow rates and heat fluxes.

2. Experimental set-up

2.1. Test rig description

Figure 1 illustrates the experimental test rig employed in this study. The apparatus consisted of a horizontal open channel with a square cross-section, fabricated from transparent polycarbonate, measuring $750\,cm$ in length and $17\,cm$ in both width and height. The test section was located at the midpoint of the channel, where the annular fin heat sink samples were mounted. Four configurations of annular fin heat sinks were examined: (i) a fin with a constant cross-section, (ii) a fin with a uniform cross-sectional area and a stepped profile, (iii) a modified stepped with triangular tip geometry, and (iv) a fin with a non-uniform triangular cross-section, and they were symbolized, such as: sample 1, sample 2, sample 3, and sample 4, respectively. Photographic images and schematic diagrams of the tested heat sink samples are provided in Fig.2. A cartridge-type electrical heater was embedded at the center of each heat sink to serve as the heat source. The heater had a rated power of $200W$ and dimensions of $8\,mm$ in diameter and $100\,mm$ in length. It was connected to an electrical circuit comprising a variac for regulating the power input, along with an ammeter and a voltmeter device for monitoring the supplied current and voltage. To establish the desired airflow, a variable-speed centrifugal blower was employed. The airflow passed uniformly through the test section, where the heat sinks were installed. A digital manometer was used to record the pressure drop across the heat sink in the working section, enabling evaluation of the thermo-hydraulic performance. Temperature measurements were acquired using a data acquisition (DAQ) system with eight channels, enabling simultaneous recording at eight locations within the test section. Figure 3 presents a schematic diagram of the complete test rig. The resolution and accuracy values presented in Table 1 are based on the manufacturers' specifications and were verified during calibration before experimentation.

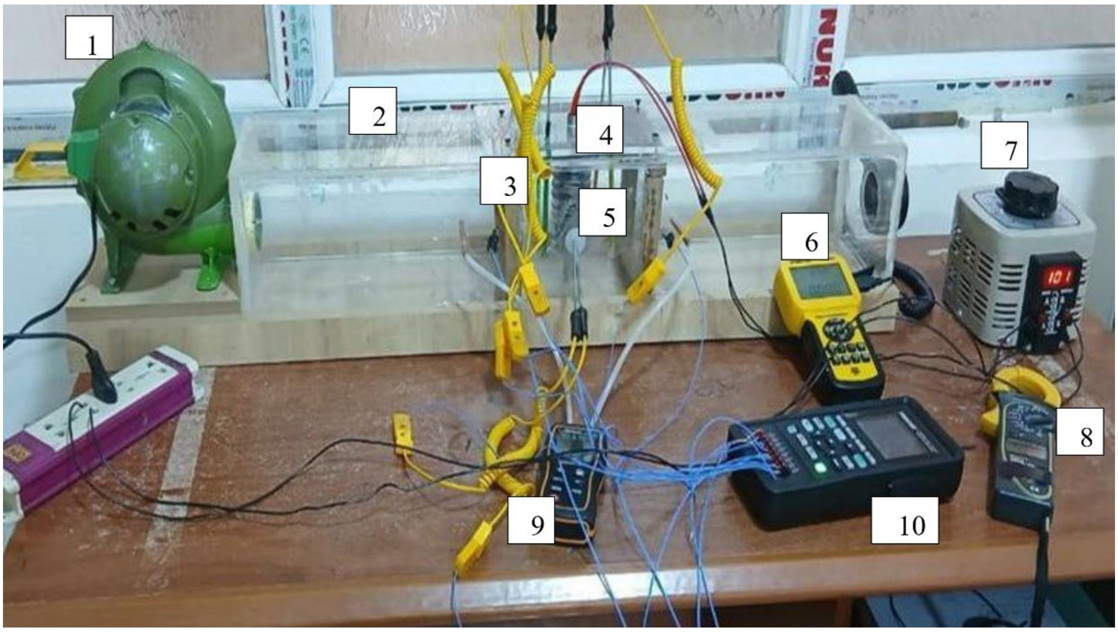

Fig.1. Photo of the test rig used, where: 1 – Centrifugal blower, 2 – Open channel, 3 – Thermocouples, 4 – Working space, 5 – Heat sink, 6 – Anemometer, 7 – Variac, 8 – Multimeter clamp meter, 9 – Digital manometer.

Table 1. The accuracy and resolution of measurement devices.

Device name	Accuracy	Resolution
Hantak-8 Data acquisition (DAQ) type HTM208B-EU	$\pm 0.2\%\,°C$	$0.1°C$
BTMETER Anemometer type BT846A	$\pm 0.01\,m/s$	$0.1\,m/s$
SNDWAY digital manometer type SW-512A	$\pm(1-2)\%\,Pa$	$0.5\%\,Pa$
Multimeter clamp meter	$\pm 0.1\%\,V$ $\pm 0.1\%\,A$	$\pm 1.2\%\,V$ $\pm 2.5\%\,A$

a)

b)

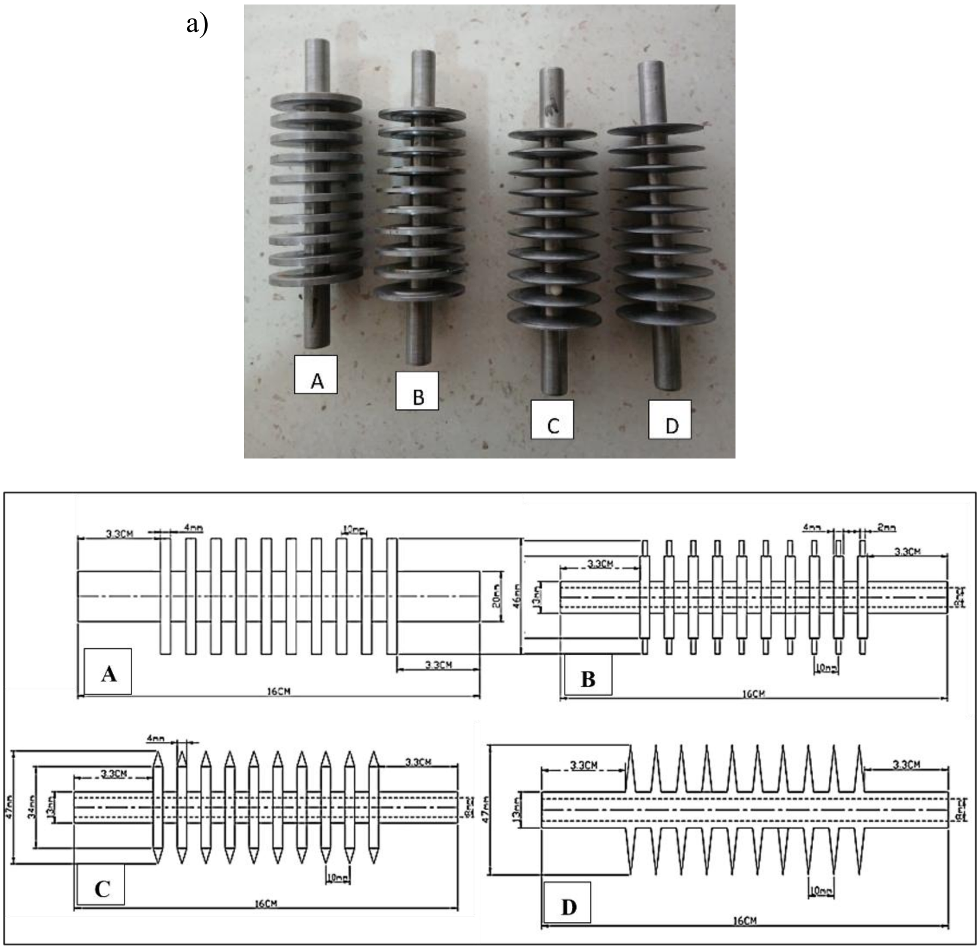

Fig.2. Annular fin heat sink configurations investigated in this study: a) Photo of heat sink, b) Schematic diagram of heat sinks: (A) sample 1, (B) sample 2, (C) sample 3, (D) sample 4.

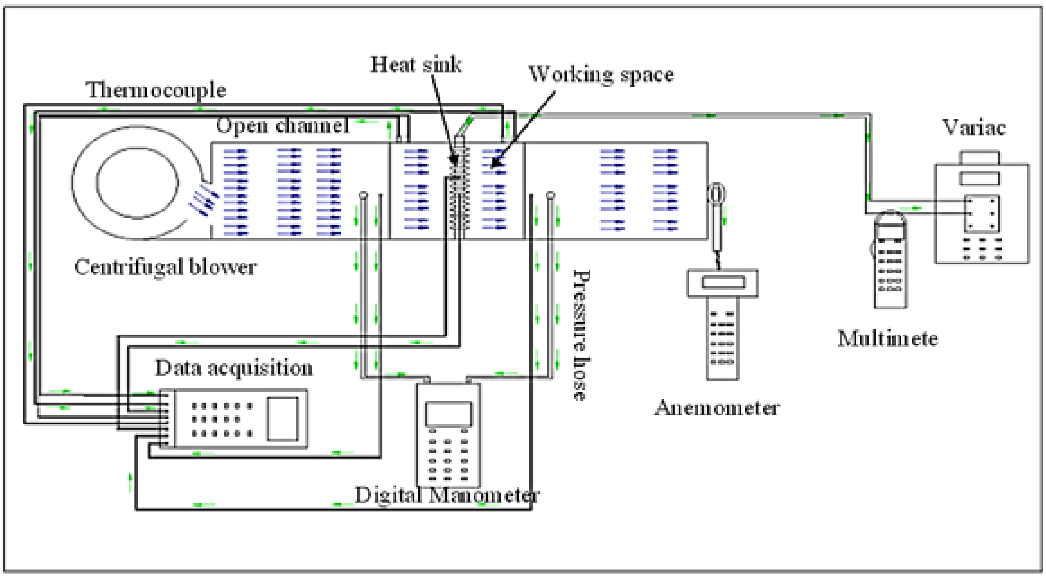

Fig.3. Schematic diagram of the test rig.

2.2. Uncertainty for measurement devices

In any experimental measurement, absolute accuracy is unattainable because every instrument and method has inherent limitations. These limitations stem from factors such as instrument precision, calibration errors, environmental variations, and human observation. The uncertainty in the present study was evaluated using Eq.(2.1), as suggested by [23]. It is expressed as:

$$w_r = \left[\left(\frac{\partial r}{\partial x_1} w_1 \right)^2 + \left(\frac{\partial r}{\partial x_2} w_2 \right)^2 + \ldots \left(\frac{\partial r}{\partial x_n} w_n \right)^2 \right]^{1/2} . \tag{2.1}$$

The uncertainty values for each device were calculated based on its accuracy and resolution, and they are presented in Tab.2.

Table 2. The uncertainty of the measurement devices used.

Device name		Uncertainty [%]
Hantak-8 Data acquisition (DAQ) type HTM208B-EU		± 0.7
BTMETER Anemometer type BT846A		± 0.015
SNDWAY digital manometer type SW-512A		± 2.6
Multimeter clamp meter	Voltmeter	± 2.2
	Ammeter	± 10.2

The total relative uncertainty calculated by Eq.(2.1) is $\pm 10.78\%$.

2.3. Experiment procedure

The experiments were conducted according to a systematic procedure to ensure accurate, reproducible measurements. The steps are summarized as follows:

a. Setup Preparation: The heater element was connected to the electrical circuit, and thermocouples were installed at their designated locations within the test section. The proper functioning of all components, including the blower, measurement devices, and data acquisition system, was verified prior to testing.
b. Initial Power Supply: The test rig was supplied with an initial power input of $100W$ and allowed to operate until the heat sink reached steady-state thermal conditions.
c. Airflow Initiation: The blower was started at an initial airflow velocity of $1 m/s$ and the system was allowed to stabilize until the heat sink cooled and achieved steady-state conditions under forced convection.
d. Data Acquisition: Temperature measurements at eight points within the test section were recorded simultaneously using an 8-channel data acquisition (DAQ) system. The pressure drop across the heat sink was measured with a digital manometer, while electrical input parameters (voltage and current) were monitored with an ammeter and a voltmeter.
e. Repetition for All Conditions: The preceding steps were repeated for all selected combinations of airflow velocities (2, 4 and $6 m/s$) and power input levels (13, 26 and $39W$) to evaluate the thermo-hydraulic performance of the annular fin heat sinks. Each condition was tested multiple times to ensure reproducibility and consistency in measurements.

2.4. Calculation

When an electrical element is supplied with power, it dissipates the energy in the form of Heat, expressed mathematically as [24]:

$$P = V \times I \ . \tag{2.2}$$

The Heat dissipated from the annular fin heat sink to the airflow within the open channel is determined as [24]:

$$Q = \dot{m} c_p \left(T_{out} - T_{in} \right) . \tag{2.3}$$

The convective heat transfer coefficient is evaluated based on Newton's law of cooling and is expressed as[24]:

$$h = \frac{Q}{A_t \left(T_b - T_\infty \right)} . \tag{2.4}$$

The term A_t denotes the total heat sink surface area for heat exchange, defined as the sum of the finned and unfinned areas, and is calculated as [25]:

$$A_t = A_f + A_{no\_fin} , \tag{2.5}$$

where:

$$A_f = N_f \times 2\pi \left(d_t^2 - d_b^2 \right) + \pi d_t t , \tag{2.6}$$

and:

$$A_{no_{fin}} = \pi d_t L - N_f \times t . \tag{2.7}$$

The Reynolds number (Re), which characterizes the airflow regime, is defined as the ratio of inertial to viscous forces, and is expressed as:

$$Re = \frac{\rho U d_h}{\mu} , \tag{2.8}$$

where:

$$d_h = \frac{4 \times A_p}{P_e} . \tag{2.9}$$

Accordingly, A_p and P_e are determined as:

$$A_p = W^2 - \left[N_f d_e t + \left(L d_b - N_f t \right) \right] , \tag{2.10}$$

and:

$$P_e = 4W + \left[\pi\left(d_b\left(L - N_f t\right) + N_f \pi\left(d_e - d_b\right) + \pi d_e t\right)\right], \tag{2.11}$$

$$Nu = \frac{h \times d_h}{k}. \tag{2.12}$$

3. Results and discussion

To examine the thermal and flow performance of annular fins, four distinct heat sink configurations were analyzed. These configurations included (i) a fin with a constant cross-section, (ii) a fin with a uniform cross-sectional area and a stepped profile, (iii) a modified fin with triangular tip geometry, and (iv) a fin with a non-uniform triangular cross-section. For clarity, these configurations were labeled as Sample 1, Sample 2, Sample 3, and Sample 4, respectively. The experimental investigation subjected each heat sink to three levels of electrical input power (13, 26 and $39W$) and three airflow velocities (2, 4 and $6\,m/s$). To obtain accurate experimental data, each experiment was repeated three times, and the average values were used in the data analysis. A 5% error bar was applied to the experimental data. This systematic variation yielded 36 experimental runs, providing a comprehensive assessment of the combined effects of geometric configuration, heating power, and airflow rate on the thermal-hydraulic characteristics of annular fin heat sinks. For clear presentation and interpretation of the results, the experimental cases were categorized and summarized in Tab.3. The discussion of the experimental results focused on the relationship between the Nusselt and Reynolds numbers and the associated changes in pressure drop. This evaluation provided insights into how the flow regime affects convective heat transfer performance and hydraulic resistance. By correlating these dimensionless parameters, the study provided a comprehensive assessment of the thermal-hydraulic behavior of annular fin heat sinks, clarifying the trade-off between improved heat transfer and increased flow resistance.

Table 3. Description of the working conditions.

Working condition	Symbol
P1	$P = 13\ W$
P2	$P = 26\ W$
P3	$P = 39\ W$
U1	$2\,m/s$
U2	$4\,m/s$
U3	$6\,m/s$

3.1. Impact of fin geometry on the Nusselt number

Figures 4 to 6 present the variation of the Nusselt number (Nu) with Reynolds number (Re) for the four annular heat sink geometries under three heating power levels. For four Figs.4-6 show the Nu - Re relation for the four types of annular heat sink configurations at three different heating powers, the Nu number increases monotonically with the Re number due to forced convection, primarily driven by greater flow penetration, reduced boundary-layer thickness, and stronger wake enforcements at higher Re numbers. This trend supports the hypothesis that airflow rate is the primary factor governing conductive heat transfer in these experiments. As the baseline comparison, Sample 1 (the uniform cross-section annular fin) has the lowest Nusselt number across the entire Reynolds number range. Introducing geometric discontinuities, as in the stepped fin case (Sample 2), increases heat transfer by $10-15\%$. No flow visualization was performed in this study, however, this augmentation is the result of a known fluid-mechanics phenomenon reported in the literature. It occurs due to sharp changes in surface geometry that lead to local boundary-layer separation and subsequent reattachment further downstream. The evolved shear layer and the redeveloping boundary layer decrease the mean thermal boundary-layer thickness, resulting in higher convective heat transfer. The modified stepped fin (Sample 3) further amplifies this effect, yielding Nu enhancements of approximately $20-25\%$ relative to Sample 1. The additional geometric modification increases the number and intensity of streamwise flow disturbances, thereby strengthening wake interactions and promoting more frequent boundary-layer redevelopment. These mechanisms are expected to become more effective as the Re number increases, because inertial forces increasingly dominate over viscous effects, allowing the flow to respond more strongly to geometric features.

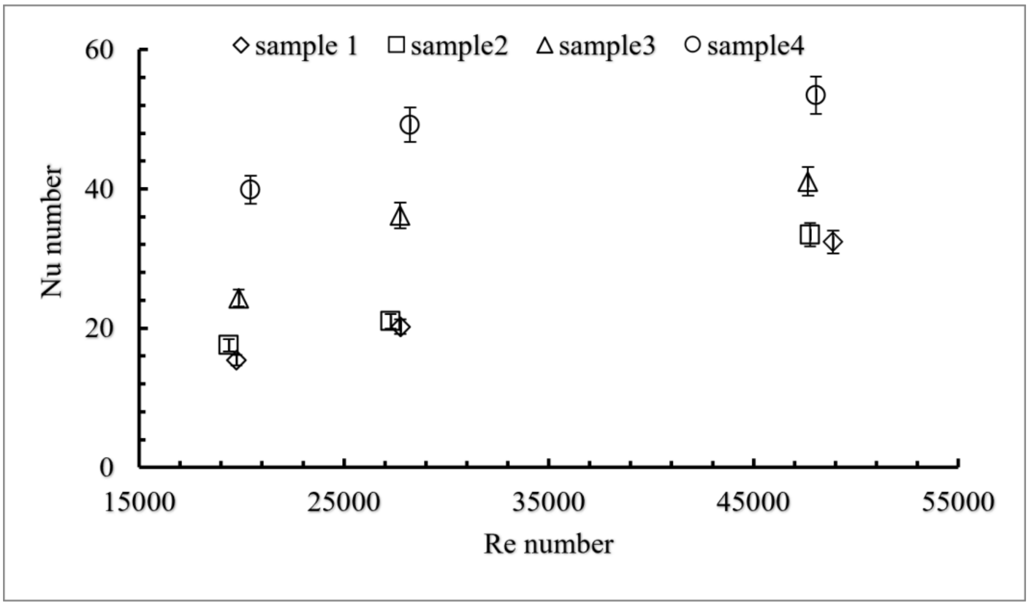

Fig.4. *Nu* Number vs. *Re* Number for four heat sink samples at P1.

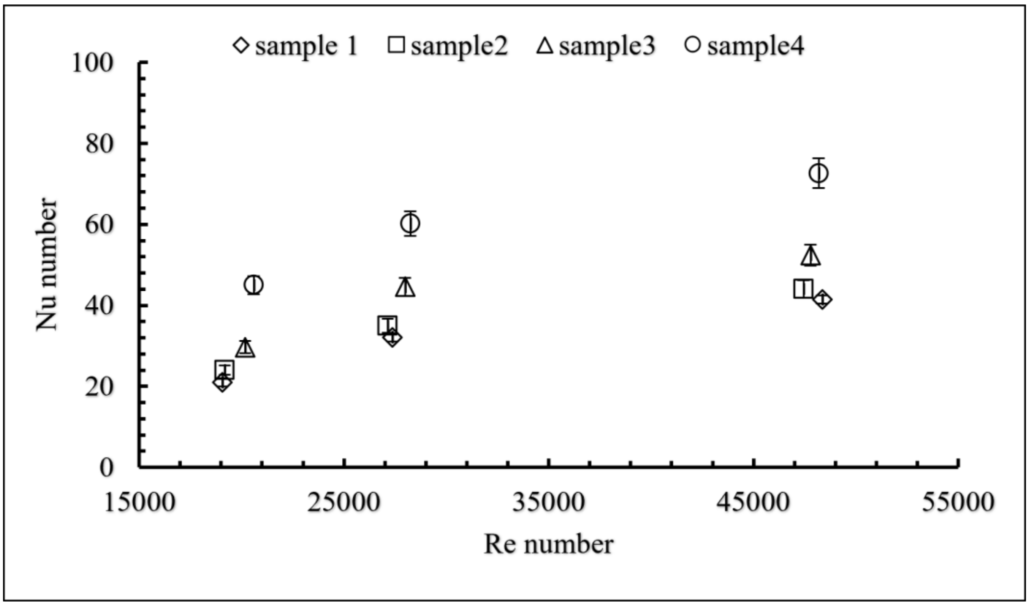

Fig.5. *Nu* Number vs. *Re* Number for four heat sink samples at P2.

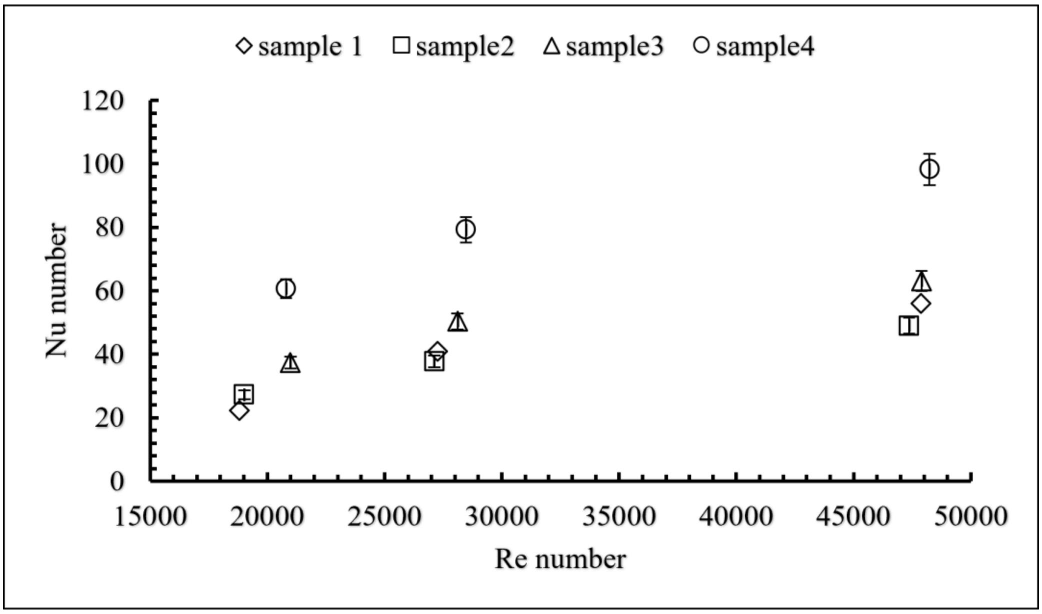

Fig.6. *Nu* Number vs. *Re* Number for four heat sink samples at P3.

3.2. Correlation relation

A unified, dimensionally consistent correlation framework was developed in SPSS to describe the *Nu* number for all annular heat sink geometries across the investigated heating powers, as expressed in Eq.(3.1). This framework is based on the behavior of the Nu number with respect to the *Re* number, as illustrated in Figures 4 to 6. The proposed model combines a *Re*-number-dependent term with a power-dependent normalization factor, while retaining geometry-specific coefficients. This approach provides excellent agreement with experimental data for all samples, with coefficients of determination exceeding 0.95:

$$Nu_i = C_i Re^{m_i} + n_i\left(\frac{P}{P_1} - 1\right). \tag{3.1}$$

It is valid for $(18000 \le Re \ge 50000)$. and $13 \le P \ge 39$, where the C_i, m_i and m_i are geometry-specific constants, their values are listed in Tab.4 for each sample.

Table 4. Geometry-specific coefficients of the unified Nusselt–Reynolds–Prandtl correlation.

Sample	C_i	m_i	n_i	R^2	Re_{min}	Re_{max}	$P_{min}\,(W)$	$P_{max}\,(W)$
1	*0.00434*	*0.826*	*6.1*	*0.952*	*18000*	*50000*	*13*	*39*
2	*0.0249*	*0.666*	*8.45*	*0.963*	*18000*	*50000*	*13*	*39*
3	*0.0812*	*0.572*	*11.35*	*0.962*	*18000*	*50000*	*13*	*39*
4	*0.4126*	*0.458*	*17.82*	*0.971*	*18000*	*50000*	*13*	*39*

3.3. Relation between *Nu* number vs. input power

Figure 7 shows how the average Nusselt number (Nu) varies with input electric power at a fixed Reynolds number of $25{,}000$. Across all annular fin configurations, Nu increases slightly with power as fin surface temperature rises, marginally enhancing convective heat transfer. Nevertheless, the weak power dependence confirms that the heat transfer process is dominated by forced convection, with airflow conditions and fin geometry as the primary controlling factors. Compared with the constant cross-section annular fin (Sample 1), variable cross-section fins exhibit significantly higher Nusselt numbers. The stepped, modified stepped, and triangular fins enhance Nu by approximately $10-15\%$, $20-25\%$ and $30-35\%$, respectively. This superior performance stems from both thermal and fluid-dynamic mechanisms. From a conduction perspective, variable cross-section fins promote a more uniform temperature distribution along the fin length, allowing a greater portion of the fin surface to participate effectively in heat transfer. From a convective standpoint, gradual or discrete changes in fin thickness locally accelerate airflow and increase near-wall velocity gradients, thinning the thermal boundary layer and enhancing convective heat transfer coefficients. As a result, variable cross-section fins achieve greater heat transfer enhancement than constant cross-section fins, and increasing input power does not alter the relative ranking of the fin geometries.

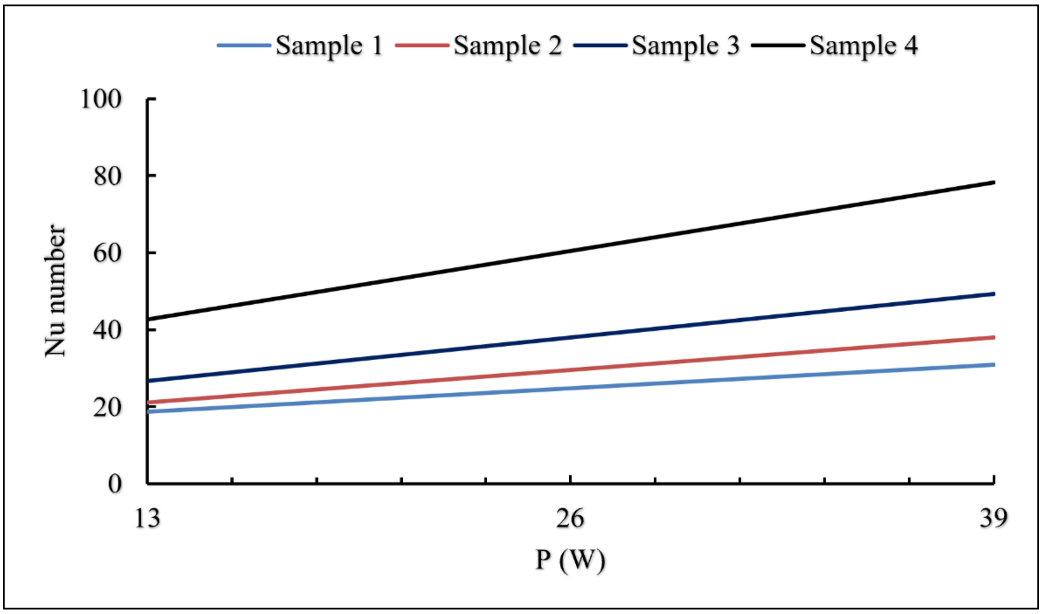

Fig.7. Variation of Nusselt number with input electric power.

3.4. Impact of fin geometry on the pressure drop

Figures 8 to 10 illustrate the pressure drop (ΔP) response of four annular fin heat-sink configurations as a function of Reynolds number (Re) at three power levels $(\mathrm{P1-P3})$. In all cases, ΔP increases steadily with Re. At low Re, as shown in Fig.8 (representing the lowest power level), the curves rise nearly linearly, indicating that viscous losses dominate. As Re increases (Fig.9), the curvature of the curves becomes more pronounced due to growing inertial contributions (form drag). At the highest velocities shown in Fig.9, the superliner increase indicates that the Forchheimer (inertial) term primarily controls the pressure drop. Across Figures 7 to 9, varying electrical power at fixed Re results in only minor vertical offsets, consistent with slight property changes due to surface temperature. At the same time, velocity (and thus Re) remains the main factor influencing ΔP. Using the constant cross-section fin (Sample 1) as a baseline, the stepped and modified stepped designs demonstrate higher ΔP across the entire range of Re presented in Figs 8 to 10, reflecting stronger flow separation and reattachment. Quantitatively, the stepped fin (Sample 2) shows an increase in pressure drop of approximately $6-10\%$ at low Re (Fig.8), $12-20\%$ at mid Re (Fig.9), and $18-28\%$ at high Re (Fig.10) compared to Sample 1. The modified stepped fin (Sample 3) amplifies these effects, resulting in the most significant increases: $10-15\%$ at low Re (Fig.8), $20-30\%$ at mid Re (Fig.8), and $30-45\%$ at high Re (Fig.10). These increases align with sharper streamwise discontinuities and more significant wake interactions, which elevate form drag at higher inertial levels. In contrast, the non-uniform triangular fin (Sample 4) redistributes material toward its base and reduces blockage at the tip. In Figs 7 to 9, it incurs only a modest penalty compared to the baseline: $3-7\%$ at low Re (Fig.8), $8-15\%$ at mid Re (Fig.9), and $12-22\%$ at high Re (Fig.10). This positions Sample 4 between the baseline and the stepped variants in terms of flow resistance, indicating that tapering can reduce large recirculation zones while still enhancing local shear.

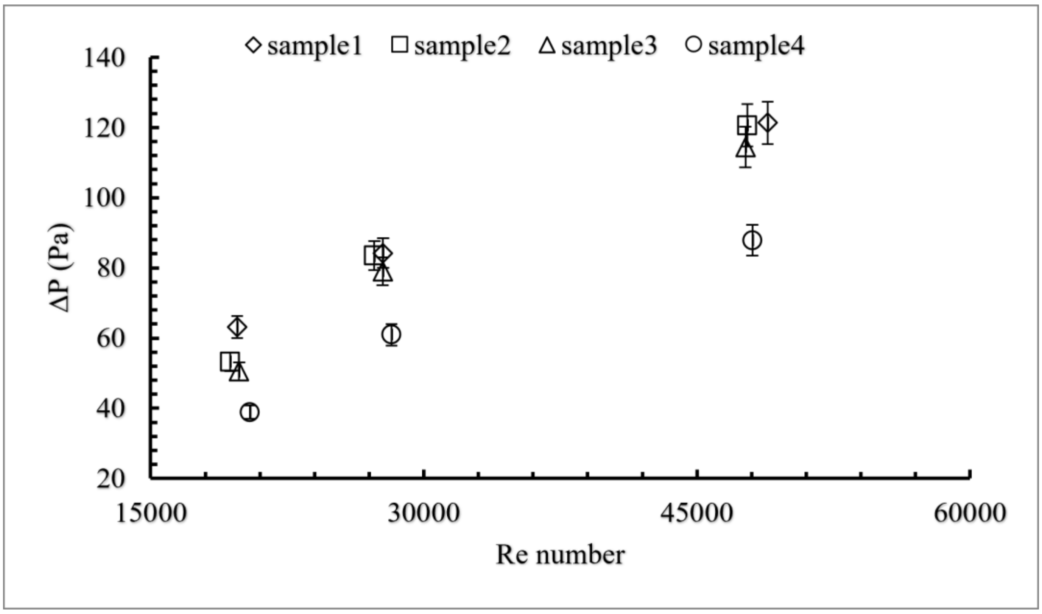

Fig.8. ΔP vs. Re number for four heat sink samples at P1.

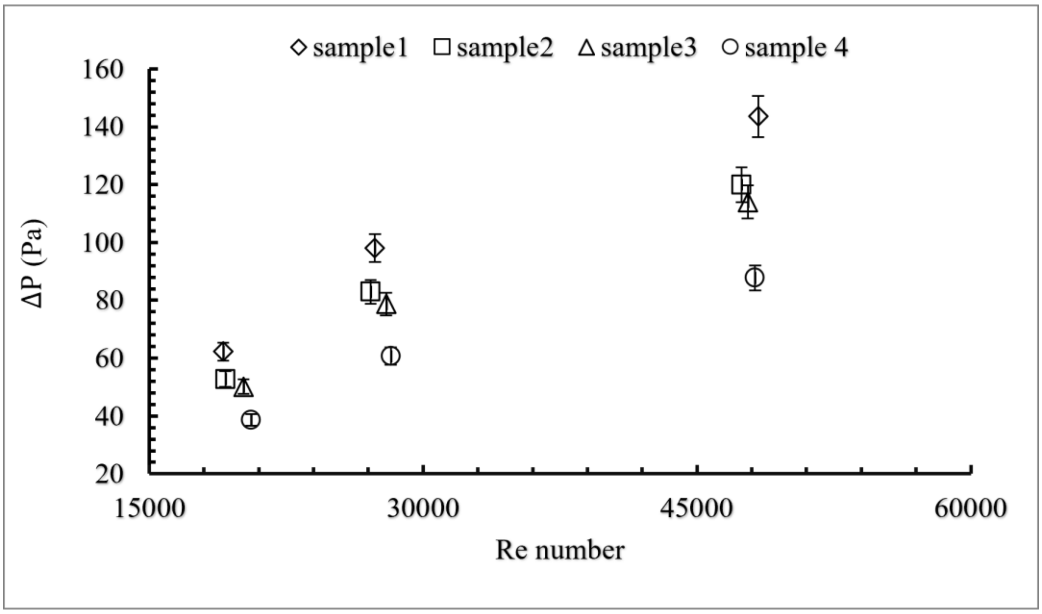

Fig.9. ΔP vs. Re number for four heat sink samples at P2.

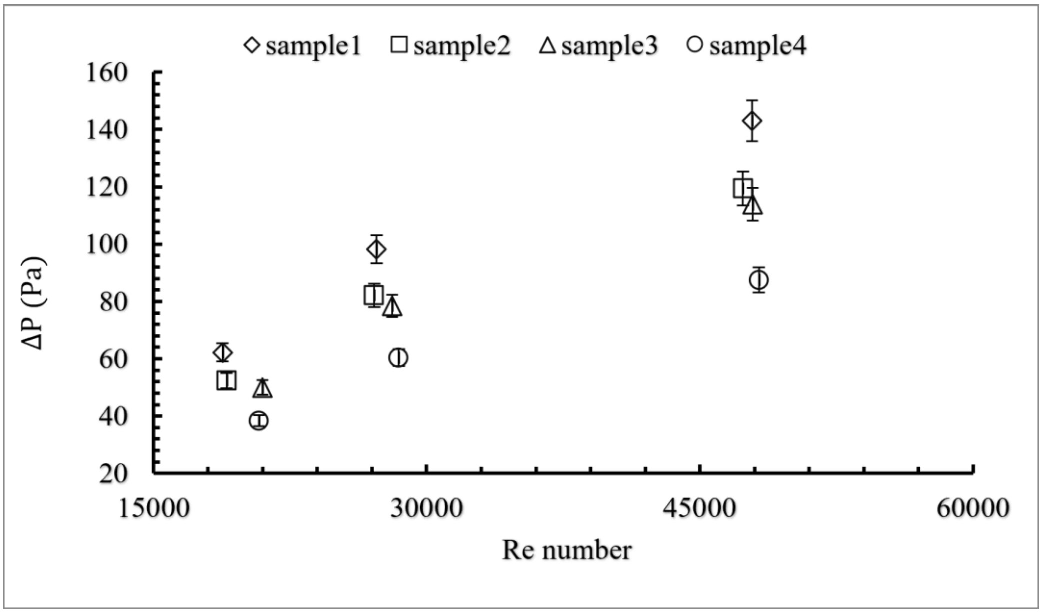

Fig.10. ΔP vs. Re number for four heat sink samples at P3.

4. Validation the fin design

The constant-cross-section annular fin (Sample 1) was validated using the dimensionless temperature formulation proposed by Brown [5]. The analytical solution, expressed in terms of the temperature ratio $\left(\frac{T_{R_o}-T_\infty}{T_{R_b}-T_\infty}\right)$, was given by:

$$\frac{T_{R_o}-T_\infty}{T_{R_b}-T_\infty}=\frac{I_0\left(mR_o\right)+\gamma K_0\left(mR_o\right)}{I_0\left(mR_b\right)+\gamma K_0\left(mR_b\right)}, \tag{4.1}$$

where:

$$\gamma=\frac{\frac{h}{mk}I_0\left(mR_o\right)+I_1\left(mR_o\right)}{K_1\left(mR_o\right)-\frac{h}{mk}K_o\left(mR_o\right)}, \tag{4.2}$$

and:

$$m=\sqrt{\frac{2h}{k\delta}}. \tag{4.3}$$

Using EES software, Eq.(4.1) was solved by applying the required experimental data, including h, k, R_o, R_b, δ and T_∞. The analytical predictions were then compared with the corresponding experimental measurements. As shown in Fig.1, good agreement was observed over the investigated Reynolds number range, with the maximum deviation between analytical and experimental results not exceeding approximately 2%, confirming the reliability of Brown's model for the present configuration.

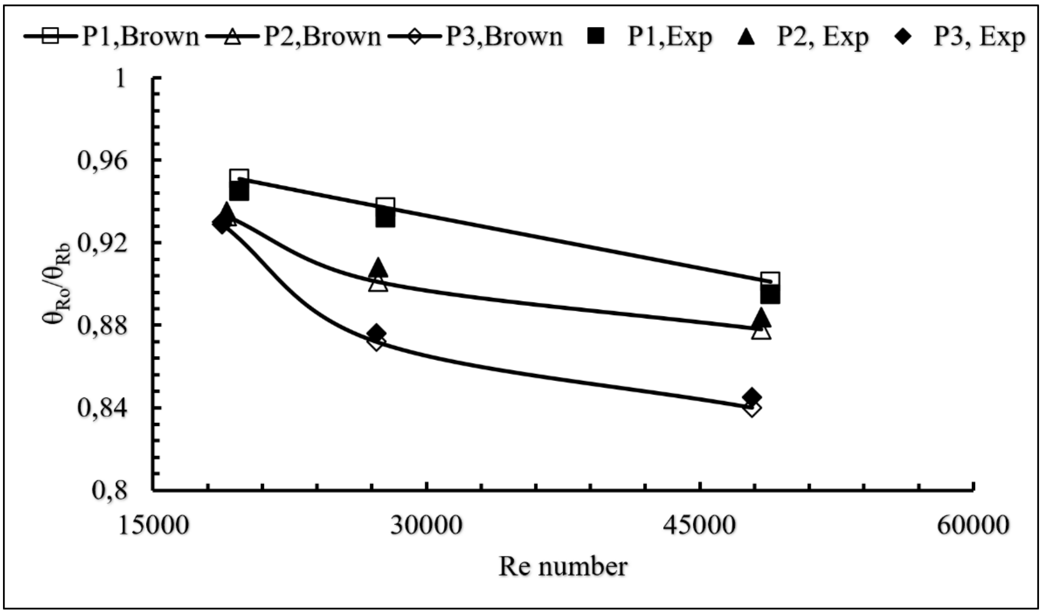

Fig.11. Validation of the analytical method against experimental results for sample 1.

5. Conclusions

Across the 36 test conditions, both the Nusselt number (Nu) and the pressure drop (ΔP) increased with Reynolds number (Re) number for four heat sink samples at for all annular fin geometries. However, the rate and magnitude of these changes varied significantly across fin shapes. Geometries designed to deliberately disturb the boundary layer, such as stepped, modified stepped, and triangular fins, exhibited steeper slopes in the *Nu–Re* relationship compared to the baseline with a constant cross-section. This confirms the importance of controlled separation and wake mixing in enhancing convective heat transfer. At high Reynolds numbers, the triangular fin provided the most significant thermal enhancement, increasing Nu by approximately $30-35\%$ relative to the baseline. The modified stepped and stepped fins achieved increases of about $20-25\%$ and $10-15\%$, respectively. The results for ΔP and Re showed the expected increase in flow resistance with rising Re, with inertial effects (form drag) being dominant at the highest velocities. Compared to the baseline, the pressure drop penalty was most significant for the modified stepped fin, which showed increases of $30-45\%$ at high Re, followed by the stepped fin, which showed increases of $18-28\%$. In contrast, the triangular fin experienced a more moderate increase in pressure drop, ranging from 12% to 22%.

Additionally, geometry-dependent correlation equations have been proposed for the four annular heat sink configurations using a standard dimensionally consistent formulation. They can thus be used to predict Nu over the range of operating conditions considered confidently. The predictive accuracy of the correlations presented was relatively good, having R^2 values of above 0.95 for everything. Additionally, an analytical model of the constant cross-section annular fin (Sample 1) derived from Brown's dimensionless temperature formulation agreed very well with experimental results with a maximum deviation of around 2%.

Acknowledgment

The authors would like to express their sincere gratitude to the Heat Transfer Laboratory, Engineering Technical College, Kirkuk, for providing the necessary facilities, technical support, and experimental resources that made this research possible. The assistance and cooperation of the laboratory staff during the experimental work are deeply appreciated.

Nomenclature

A_f – fin area
A_{no-fin} – smooth plate area
A_p – plate area
A_t – total area
C_p – specific Heat
d_b – base diameter
d_h – hydraulic diameter
d_t – tip diameter
h – coefficient of convection heat transfer
I – current
I_0, I_1 – Bessel functions
k – thermal conductivity
K_0, K_1 – Bessel functions
L – width of the heat sink
$\dot{m}$ – mass flow rate
N_f – number of fins
Nu – Nusselt number
P – power
Pe – perimeter
Q – heat transfer rate
R_b – base radius
Re – Renoyldes number
R_o – tip radius
T_b – bulk temperature
T_{in} – inlet temperature
T_{out} – outlet temperature
T_{Rb} – base temperature
T_{Ro} – tip temperature
T_∞ – fluid temperature
V – voltage
w – uncertainity
W – width of the heat sink cover
δ – thickness
μ – viscosity
θ – T-T_∞

References

[1] Abbas E.F. (2024): *An overview of heat sink technology*.– International Journal of Applied Mechanics and Engineering, vol.29, No.4, pp.1-23, doi:10.59441/ijame/192127

[2] Abbas E.F., Jassim A.H., and Salem T.K. (2025): *Examining the impact of conical fin shape on hydrothermal characteristics*.– International Journal of Heat and Technology, vol.43, No.1, pp.29-38, doi:10.18280/ijht.430104

[3] Kraus A.D., Aziz A., and Welty J. (2001): *Extended Surface Heat Transfer*.– John Wiley & Sons, Inc., doi:10.1002/9780470172582

[4] Abbas E.F., Jassim A.H., and Salem T.K. (2023): *Review of the fin optimization in the heat sink design*.– International Review of Mechanical Engineering, vol.17, No.10, doi:10.15866/ireme.v17i10.23824.

[5] Brown A. (1965): *Optimum dimensions of uniform annular fins*.– Journal of Heat and Mass Transfer, vol.8, No.4, pp.655-662, doi:10.1016/0017-9310(65)90051-7.

[6] Buccini A. and Soliman H.M. (1986): *Optimum dimensions of annular fin assemblies*.– J. Heat Transfer, vol.108, No.2, pp. 459-462, doi:10.1115/1.3246947.

[7] Lalot S., Tournier C. and Jensen M. (1999): *Fin efficiency of annular fins made of two materials.*– Int. J. Heat Mass Transfer, vol.42, No.18, pp.3461-3467, https://doi.org/10.1016/S0017-9310(99)00009-5.

[8] Mokheimer E.M.A. (2002): *Performance of annular fins with different profiles subject to variable heat transfer coefficient.*– Int. J. Heat Mass Transfer, vol.45, No.17, pp.3631-3642, https://doi.org/10.1016/S0017-9310(02)00078-9.

[9] Arslanturk C. (2005): *Simple correlation equations for optimum design of annular fins with uniform thickness.*– Appl. Therm. Eng., vol.25, No.14-15, pp.2463-2468, https://doi.org/10.1016/j.applthermaleng.2004.12.007.

[10] Naphon P. (2006): *Study on the heat transfer characteristics of the annular fin under dry-surface, partially wet-surface, and fully wet-surface conditions.*– Int. Commun. Heat Mass Transfer, vol.33, No.1, pp.112-121, https://doi.org/10.1016/j.icheatmasstransfer.2005.08.009.

[11] Sharqawy M.H. and Zubair S.M. (2007): *Efficiency and optimization of an annular fin with combined heat and mass transfer – an analytical solution.*– Int. J. Refrigeration, vol.30, No.5, pp.751-757, https://doi.org/10.1016/j.ijrefrig.2006.12.008.

[12] Aziz A. and Fang T. (2011): *Thermal analysis of an annular fin with (a) simultaneously imposed base temperature and base heat flux and (b) fixed base and tip temperatures.*– Energy Convers. Manage., vol.52, No.7, pp.2467-2478, https://doi.org/10.1016/j.enconman.2011.02.004.

[13] Nagarani N., Mayilsamy K. and Murugesan A. (2012): *Fin effectiveness optimization of elliptical annular fins by genetic algorithm.*– Procedia Eng., vol.38, pp.2939-2948, https://doi.org/10.1016/j.proeng.2012.06.343.

[14] Moinuddin A., Sharqawy M.H. and Zubair S.M. (2012): *Heat and mass transfer from annular fins of different cross sectional area. Part II. Optimal dimensions of fins.*– Int. J. Refrigeration, vol.35, No.2, pp.377-385, https://doi.org/10.1016/j.ijrefrig.2011.11.003.

[15] Huang C.H. and Chung Y.L. (2014): *The determination of optimum shapes for fully wet annular fins for maximum efficiency.*– Appl. Therm. Eng., vol.73, No.1, pp.438-448, https://doi.org/10.1016/j.applthermaleng.2014.07.071.

[16] Kundu B., Lee K.S. and Campo A. (2015): *An ease of analysis for optimum design of an annular step fin.*– Int. J. Heat Mass Transfer, vol.85, pp.221-227, https://doi.org/10.1016/j.ijheatmasstransfer.2015.01.111.

[17] Kundu B. and Lee K.S. (2016): *A proper analytical analysis of annular step porous fins for determining maximum heat transfer.*– Energy Convers. Manage., vol.110, pp.469-480, https://doi.org/10.1016/j.enconman.2015.09.037.

[18] Chen H.T., Chiu Y.J., Liu C.S. and Chang J.R. (2017): *Numerical and experimental study of natural convection heat transfer characteristics for vertical annular finned tube heat exchanger.*– Int. J. Heat Mass Transfer, vol.109, pp.378-392, https://doi.org/10.1016/j.ijheatmasstransfer.2017.01.122.

[19] Yuan S., Cheng W.L., Nian Y.L., Zhong Q., Fan Y.F. and He J. (2017): *Evaluation of prediction methods for heat transfer coefficient of annular flow and a novel correlation.*– Appl. Therm. Eng., vol.114, pp.10-23, https://doi.org/10.1016/j.applthermaleng.2016.11.170.

[20] Ren K., Yuan W., Miao Z. and Yang B. (2020): *Influence of inlet/outlet arrangement on flow boiling of a parallel strip fin heat sink.*– Appl. Therm. Eng., vol.176, art.115061, https://doi.org/10.1016/j.applthermaleng.2020.115061.

[21] Umrao Sarwe D. and Kulkarni V.S. (2021): *Differential transformation method to determine heat transfer in annular fins.*– Heat Transfer, vol.50, No.8, pp.7678-7693, https://doi.org/10.1002/htj.22261.

[22] Tahrour F., Ahmad H., Ameur H., Saeed T., Abu-Zinadah H. and Menni Y. (2023): *3D numerical study and comparison of thermal-flow performance of various annular finned-tube designs.*– J. Ocean Eng. Sci., vol.8, No.3, pp.294-307, https://doi.org/10.1016/j.joes.2022.02.009.

[23] Sun J., Xie X., Li J., Zhong M., Zhang R. and Wang Y. (2025): *Numerical and experimental study of heat transfer performance of the array orifice microjet heat sink with different structures.*– Appl. Therm. Eng., vol.261, art.125164, https://doi.org/10.1016/j.applthermaleng.2024.125164.

[24] Shah R.K. and Sekuli D.P. (2003): *Fundamentals of Heat Exchanger Design.*– John Wiley & Sons, Inc., https://doi.org/10.1002/9780470172605.

Received: January 13, 2026

Revised: April 8, 2026